Int J Earth Sci (Geol Rundsch) (2017) 106:501–515
DOI 10.1007/s00531-016-1387-z

ORIGINAL PAPER

Ordovician magmatism in the Lévézou massif (French Massif Central): tectonic and geodynamic implications

Caroline Lotout[1] · Pavel Pitra[1,2] · Marc Poujol[1] · Jean Van Den Driessche[1]

Received: 22 March 2016 / Accepted: 5 August 2016 / Published online: 13 August 2016

Abstract New U–Pb dating on zircon yielded ca. 470 Ma ages for the granitoids from the Lévézou massif in the southern French Massif Central. These new ages do not support the previous interpretation of these granitoids as syn-tectonic intrusions emplaced during the Late Devonian-Early Carboniferous thrusting. The geochemical and isotopic nature of this magmatism is linked to a major magmatic Ordovician event recorded throughout the European Variscan belt and related to extreme thinning of continental margins during a rifting event or a back-arc extension. The comparable isotopic signatures of these granitoids on each side of the eclogite-bearing leptyno-amphibolitic complex in the Lévézou massif, together with the fact that they were emplaced at the same time, strongly suggest that these granitoids were originally part of a single unit, tectonically duplicated by either isoclinal folding or thrusting during the Variscan tectonics.

Keywords Variscan · Orthogneiss · Geochronology U/Pb · Ordovician · Geochemistry

Electronic supplementary material The online version of this article (doi:10.1007/s00531-016-1387-z) contains supplementary material, which is available to authorized users.

✉ Caroline Lotout
caroline.lotout@univ-rennes1.fr

[1] UMR CNRS 6118, Géosciences Rennes, OSUR, Université, Rennes 1, 35042 Rennes Cedex, France

[2] Česká Geologická Služba, Klárov 3, 118 21 Prague 1, Czech Republic

Introduction

Variscan tectonics during the Late Devonian-Early Carboniferous is classically viewed as the result of a continental collision following oceanic subduction (e.g., Dewey and Burke 1973). The close association of strongly deformed high-pressure/high-temperature (HP/HT) metamorphic mafic and felsic rocks within the so-called leptyno-amphibolitic complex (LAC; Forestier 1961; Lasnier 1968; Forestier et al. 1973; Santallier et al. 1988) is considered to be a tectonic mélange s.l. that formed during the closure of one or several oceans previously separating the continental blocks (e.g., Bard et al. 1980; Matte and Burg 1981; Pin and Vielzeuf 1983; Matte 1986). Different geodynamic interpretations have been proposed that commonly involve two major continents separated by magmatic arcs or several micro-blocks that resulted from the extreme stretching of the continental margins prior to oceanic subduction (e.g., Bard et al. 1980; Matte and Burg 1981; Matte 1986, 1991; Pin 1990; Franke 2006; Ribeiro et al. 2007; Martínez Catalán et al. 2009; Lardeaux 2014; Schulmann et al. 2014). All these interpretations agree, however, on the fact that the Variscan belt resulted from the final collage of two supercontinents, Laurussia to the north and Gondwana to the south (Fig. 1). The Early Paleozoic pre-orogenic extensional event is recorded across the entire Variscan belt by the formation of large Cambro-Ordovician sedimentary basins (e.g., Young 1990; Linnemann et al. 2004) and massive bimodal magmatism (e.g., Pin 1990; Pin and Marini 1993; Abati et al. 1999; Crowley et al. 2000; Sánchez-García et al. 2003, 2008). Among the most typical examples are the porphyritic granitic and rhyolitic orthogneisses with emplacement ages clustering between 490 and 450 Ma (e.g., Helbing and Tiepolo 2005; Solá et al. 2008; Montero et al. 2009; Ballèvre et al. 2012; Talavera et al. 2013; Del Greco et al. 2016 and references therein).

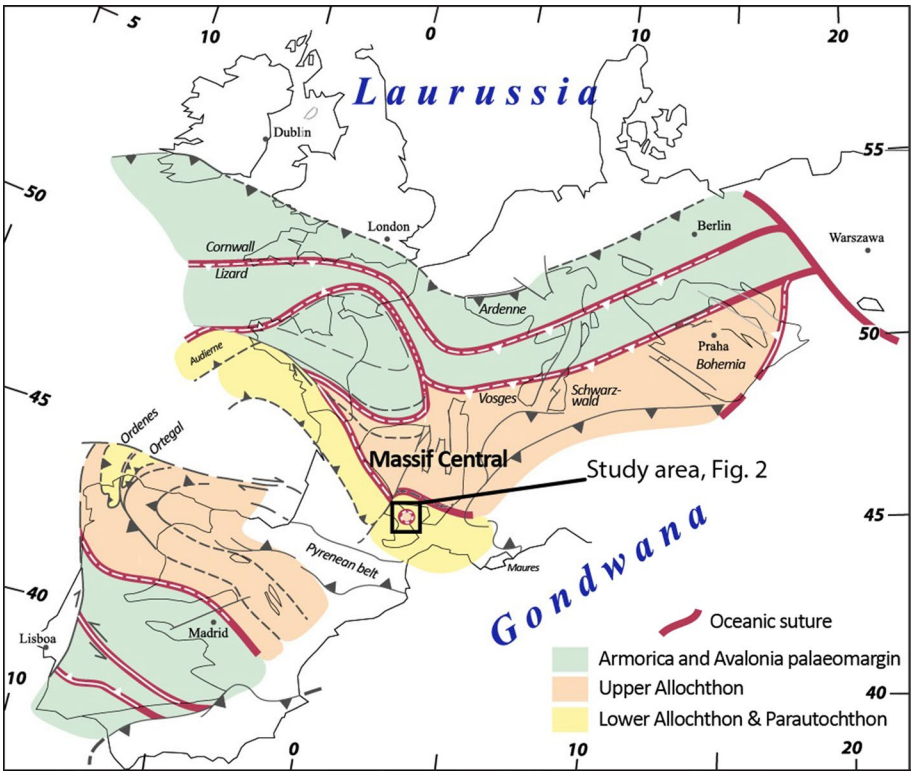

Fig. 1 Tectonic sketch of the Variscan belt (after Ballèvre et al. 2009). The study area in the French Massif Central is indicated

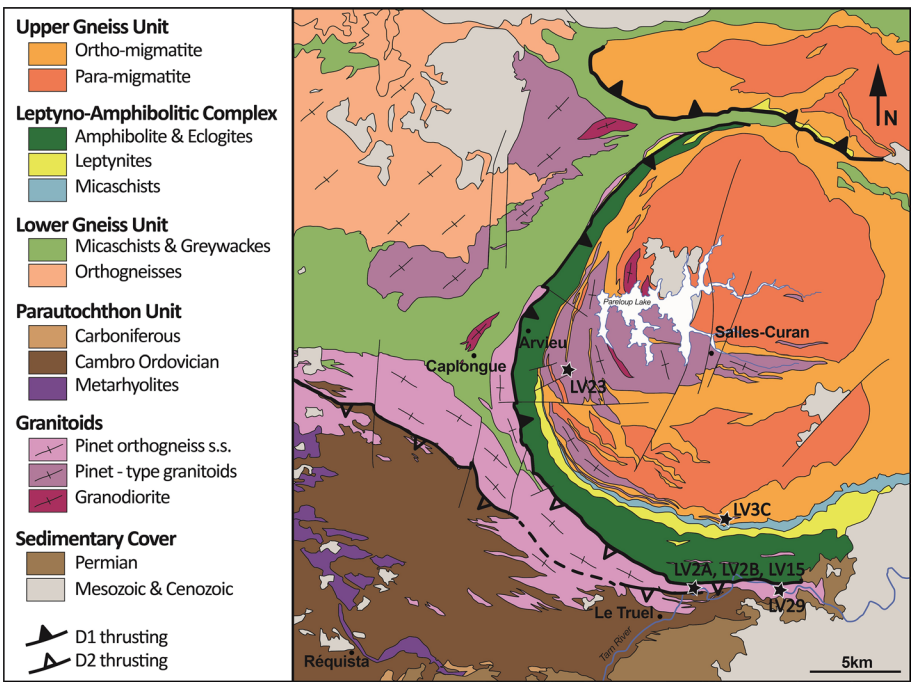

Fig. 2 Simplified geological map of the Lévézou Massif (modified from Delor et al. 1989; Guérangé-Lozes et al. 1995; Duguet and Faure 2004). *Black stars* indicate sample locations

In the southern French Massif Central, the Lévézou is a dome-shaped massif that comprises migmatitic paragneisses and orthogneisses in the core, surrounded by the eclogite-bearing LAC, itself surrounded by lower-grade orthogneiss and micaschists (Fig. 2). The occurrence of the LAC separating two gneissic units makes it a key area, because it typifies the Variscan architecture, in particular in the Massif Central. The external (Pinet) orthogneiss has been interpreted as a syn-kinematic intrusion, emplaced and deformed during the Late Devonian-Early Carboniferous thrusting event (Pin 1981; Burg and Teyssier 1983; Burg 1987; Dutruge and Burg 1997; Duguet and Faure

2004). The petrology and the deformation patterns of this orthogneiss, however, strongly remind those of the Caroux and Espinouse massifs (Montagne Noire) located ~50 km farther to the south, and whose protoliths were recently dated at 450–455 Ma (Roger et al. 2004; Pitra et al. 2012). This leads us to re-examine the Lévézou orthogneisses from a petrological, geochemical, geochronological and finally tectonic point of view.

Geological setting

The French Massif Central is traditionally subdivided into four Gondwana-derived units, based on their petrological characteristics: the Upper Gneiss Unit (UGU), the leptyno-amphibolitic complex (LAC), the Lower Gneiss Unit (LGU) and the parautochthon unit (PAU) (e.g., Burg and Matte 1978; Matte 1986; Ledru et al. 1989; Figs. 1, 2). Some authors refer to the Upper and Lower Gneiss Units as the upper and lower allochthon, respectively (e.g., Ballèvre et al. 2009, 2014). Classically, the LGU and UGU correspond to two continents separated by an oceanic crust (LAC) before the Carboniferous collision (e.g., Burg and Matte 1978; Matte and Burg 1981; Matte 1986, 2001). A recent study (e.g., Lardeaux 2014) has re-interpreted the Upper and Lower Gneiss Unit as an extremely thinned margin of Gondwana: UGU corresponding to the more distal blocks and LGU to the proximal ones. The LGU and the PAU display low-grade metamorphism, while the LAC and the UGU have recorded high-pressure (HP) and high-temperature (HT) metamorphism, respectively (e.g., Ledru et al. 1989). Granitoids close to the tectonic contact between the LGU and the LAC were interpreted as syntectonic intrusions (Ledru et al. 1989; Duguet and Faure 2004). The Lévézou massif comprises all of these units and represents therefore a classic example of the Variscan architecture (Fig. 2).

The LAC in the Lévézou is dominated by amphibolites with tholeiitic and calc-alkaline affinities (Nicollet 1978; Piboule 1979). It contains abundant lenses of eclogite and locally peridotite. The emplacement of the tholeiitic suite was dated at ca. 485 ± 30 Ma (U/Pb on zircon population from a trondhjemite; Pin 1979). A gabbro from the calc-alkaline suite was dated at 367 ± 10 Ma with the same method (Pin and Piboule 1988). The upper part of the LAC comprises micaschists, leucocratic paragneisses and quartzites. For Piboule (1979) and Briand et al. (1988), the magmatic signature of the LAC is that of a back-arc basin environment rather than that of an oceanic one. Pin and Piboule (1988) proposed a collision between two independent magmatic suites to account for the composite character of the LAC. Finally, Lardeaux (2014) reinterpreted the REE spectrum of the tholeiitic suite as being compatible with an ocean–continent transition zone. The age of the eclogite-facies HP event in the Lévézou massif is unknown. In the whole French Massif Central, this age is considered to be Silurian (ca. 430–400 Ma; U/Pb on zircon population, Pin and Lancelot 1982; Ducrot et al. 1983; Sm/Nd on garnet, Paquette et al. 1995; in situ U/Pb on 2 zircon grains, Berger et al. 2010). Because of the oceanic affinity of its rocks and the presence of eclogite relics, the LAC is a key unit that has been interpreted as marking the orogenic suture between the UGU and the LGU (e.g., Bard et al. 1980; Matte 1986). In the Lévézou massif, the LAC forms a conspicuous arc that separates the inner (UGU) from the outer (LGU) part of the massif. It dips steeply to the south (beneath the LGU) in the southern part of the massif, and to the east, beneath the UGU, in the western part of the massif (Fig. 2). This led to a large spectrum of tectonic interpretations (see below).

The UGU forms the core of the Lévézou massif and is composed of paragneisses and felsic orthogneisses, migmatized to various degrees. The felsic orthogneisses, termed "Pinet-type granitoids" (cf. below) in the literature, are deformed calc-alkaline S-type granites (Nicollet 1978). Mafic enclaves with some relics of HP mineral assemblages, interpreted as xenoliths, are locally found within the orthogneisses (Delor et al. 1985) whose emplacement was considered to be Carboniferous in age (e.g., Pin 1981; Burg and Teyssier 1983).

The LGU outcrops in the western part of the massif. It is composed of amphibolite-facies metasedimentary rocks, mainly micaschists, metapelitic paragneisses, and metagreywackes, intruded by several granitoid bodies. The protolith ages of the Rodez alkaline orthogneiss and the Caplongue metagranodiorite are considered to be Cambrian (U/Pb on zircon population, Lafon 1984). The granitic Pinet orthogneiss s.s. forms an elongated body mostly parallel to the contact between the LAC and the LGU (Fig. 2). Based on the analysis of the deformation patterns, Burg and Teyssier (1983) and Dutruge and Burg (1997) argued that this granite emplaced as a syntectonic laccolith. The emplacement of the granitic protolith of the Pinet orthogneiss was dated at ca. 360 Ma (Pin 1981). The combination of these two interpretations, if correct, is crucial since it linked the main episode of thrusting to the Variscan history of the Massif Central.

The PAU is the most external and less metamorphosed unit (Fig. 2). It is composed of the so-called Saint-Sernin-sur-Rance nappe, including quartzo-pelitic rocks, micaschists and quartzites with intercalated Cambrian metarhyolites (Collomb 1970; Delbos et al. 1964). The presence of a contact metamorphism was described within the PAU along the contact with the Pinet orthogneiss (Nicollet 1978).

The different tectonic interpretations of the Lévézou massif all involve a first major thrusting event,

responsible for the parallelism between foliations, lithological boundaries or major contacts, and are related to the Late Devonian-Early Carboniferous Variscan collision that followed subduction of an oceanic crust and the related eclogite-facies metamorphism. Interpretations differ on the origin of the final dome-like shape of the massif, ranging from diapirism (Burg and Teyssier 1983; Burg 1987), recumbent fold nappe (Burg et al. 1986; Duguet and Faure 2004) or extensional gneiss dome (Burg et al. 1994).

Analytical procedures

Chemical and isotopic analyses

The samples were first cleaned from any weathered material and then crushed in a jaw crusher and in an agate mortar in order to obtain a fine powder. Major and trace elements analysis were performed by inductively coupled plasma atomic emission spectrometry (ICP-AES) and inductively coupled plasma mass spectrometer (ICP-MS), respectively, at the Geochemical and Petrographical Research Center (SARM Laboratory, CNRS-CRPG) in Nancy, following the procedure described in Carignan et al. (2001).

Whole-rock Sm–Nd and Sr isotope analyses were carried out at the Geosciences Rennes Laboratory using a 7 collectors Finnigan MAT-262 mass spectrometer. For a complete procedure see Ballouard et al. (2015). The samples were analyzed together with the AMES Nd standard that yielded a mean $^{143}Nd/^{144}Nd$ ratio of 0.511973 (±4) and with the Sr standard NBS 987 with a mean $^{87}Sr/^{86}Sr$ ratio of 0.710222 (±9). Blank analyses yield values of 160 pg for Sr and 25 pg for Nd and were therefore considered to be negligible. Data are plotted using the software GCDkit (Janoušek et al. 2006).

U–Th–Pb dating

A classic mineral separation procedure has been applied to concentrate the zircon grains for U–Pb dating using the facilities available at the University of Rennes. Rocks were crushed and only the powder fraction with a diameter <250 µm has been kept. Heavy minerals were successively concentrated by Wilfley table and heavy liquids. Magnetic minerals were then removed with an isodynamic Frantz separator. Zircon grains were then handpicked under a binocular microscope. The selected grains were then embedded in epoxy mounts. The mounts were grounded and polished on a lap wheel. Zircon grains were imaged by cathodoluminescence (CL) using a Reliotron CL system equipped with a digital color camera available in Géosciences Rennes.

U–Pb geochronology of zircon grains was conducted by in situ laser ablation inductively coupled plasma mass spectrometry (LA-ICP-MS) at Géosciences Rennes using a ESI NWR193UC Excimer laser coupled to an Agilent quadripole 7700× ICP-MS equipped with a dual pumping system to enhance sensitivity. The instrumental conditions are reported in the Supplementary Table 1.

The ablated material is carried into helium and then mixed with nitrogen (Paquette et al. 2014) and argon, before injection into the plasma source. The alignment of the instrument and mass calibration was performed before each analytical session using the NIST SRM 612 reference glass, by inspecting the ^{238}U signal and by minimizing the ThO+/Th+ ratio (<0.5 %). During the course of an analysis, the signals of $^{204}(Pb + Hg)$, ^{206}Pb, ^{207}Pb, ^{208}Pb and ^{238}U masses are acquired. The occurrence of common Pb in the sample can be monitored by the evolution of the $^{204}(Pb + Hg)$ signal intensity, but no common Pb correction was applied owing to the large isobaric interference with Hg. The ^{235}U signal is calculated from ^{238}U on the basis of the ratio $^{238}U/^{235}U = 137.88$. Single analyses consisted of 20 s of background integration followed by 60-s integration with the laser firing and then a 10-s delay to wash out the previous sample. Ablation spot diameters of 20 µm with repetition rates of 4 Hz were used. Data were corrected for U–Pb and Th–Pb fractionation and for the mass bias by standard bracketing with repeated measurements of the GJ-1 zircon standard (Jackson et al. 2004). Along with the unknowns, the zircon standard 91500 (1065 Ma, Wiedenbeck et al. 1995) was measured to monitor precision and accuracy of the analyses and produced a concordia age of 1063.7 ± 4.8 Ma ($N = 27$, MSWD = 1.5) during the course of the analyses. Data reduction was carried out with the GLITTER® software package developed by the Macquarie Research Ltd. (Van Achterbergh et al. 2001). Concordia ages and diagrams were generated using Isoplot/Ex (Ludwig 2012). All errors given in Supplementary Table 2 are listed at one sigma, but where data are combined for concordia age or weighted mean calculations, the final results are provided with 95 % confidence limits. Further information on the protocol can be found in Ballouard et al. (2015).

Petrography and geochemistry

Samples with various degrees of deformation were selected, in order to check the possible influence of the deformation on the geochemical and geochronological data: two macroscopically undeformed samples (LV3C, LV23) of the Pinet-type granitoids from the inner part (UGU) of the Lévézou massif, and one undeformed sample (LV2A), one augen orthogneisses (LV2B) and one mylonite (LV15) from the

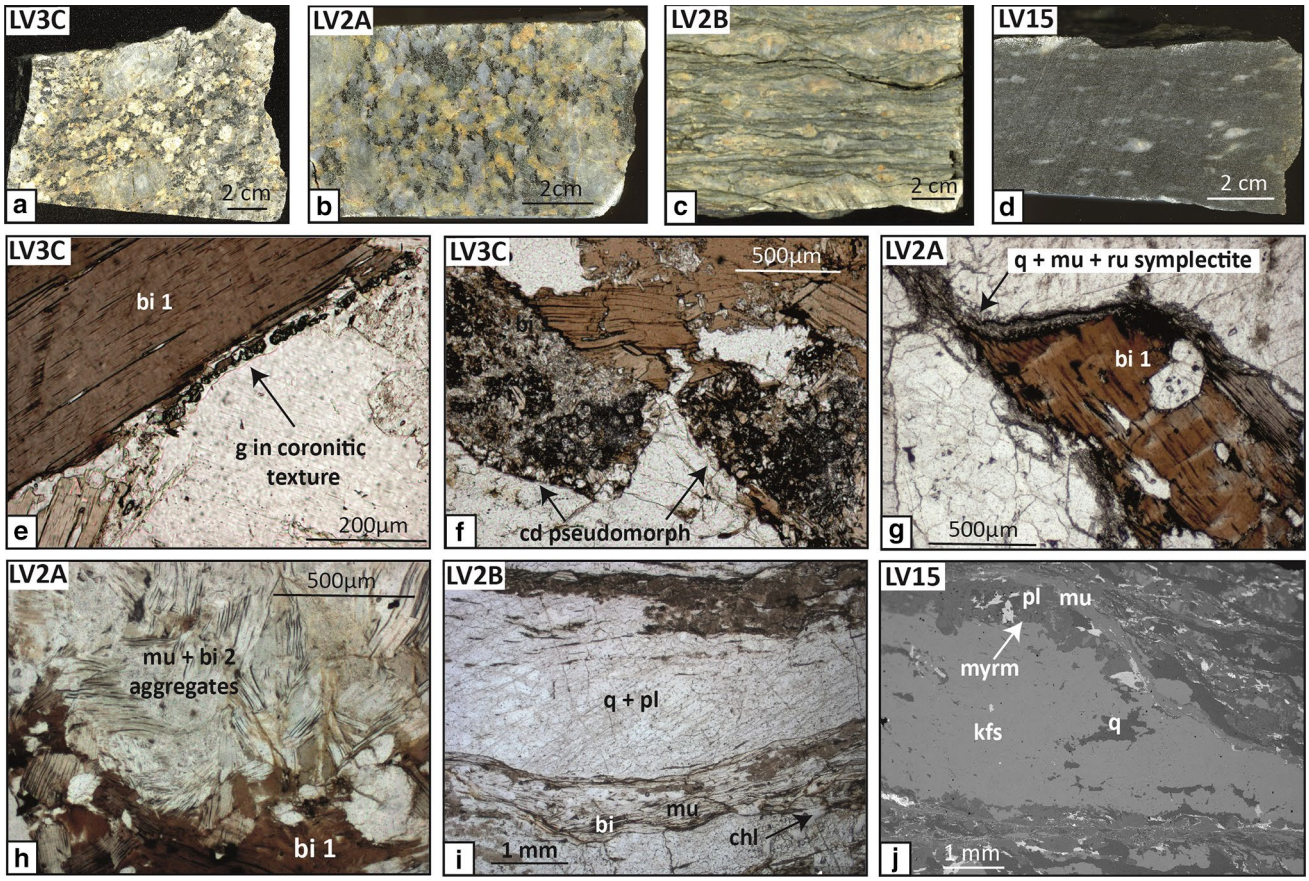

Fig. 3 **a** Undeformed porphyritic facies of the inner Pinet-type granitoid (LV3C), **b** undeformed porphyritic facies of the Pinet orthogneiss (LV2A), **c** augen orthogneiss facies of the Pinet orthogneiss (LV2B), **d** ultramylonite facies of the Pinet orthogneiss (LV15), **e** garnet corona around primary biotite (bi 1; LV3C), **f** cordierite pseudomorphed by fine-grained garnet + muscovite + kyanite in LV3C, **g** quartz + muscovite + rutile symplectite surrounding a primary biotite crystal displaying several kink-bands (LV2A), **h** muscovite and secondary biotite aggregate in LV2A, **i** chlorite, muscovite, and biotite foliation surrounding quartz, plagioclase, and K-feldspar augen in LV2B, **j** K-feldspar porphyroclast surrounded by myrmekite and muscovite-bearing foliation in LV15. *bi* biotite, *cd* cordierite, *chl* chlorite, *g* garnet, *kfs* K-feldspar, *mu* muscovite, *myr* myrmekite, *pl* plagioclase, *q* quartz, *ru* rutile

Pinet orthogneiss in the outer part (LGU) of the massif (Fig. 2).

Inner undeformed porphyritic facies

Two rock samples from the core of the Lévézou massif (LV3C, LV23, Fig. 2), although sampled at geographically distant locations (some 12 km apart), are petrographically almost identical. They represent a macroscopically undeformed isotropic coarse-grained porphyritic granite (Fig. 3a) dominated by quartz, plagioclase, K-feldspar, biotite, and muscovite. The rocks appear undeformed, but thin-section observations reveal abundant metamorphic textures. Quartz (up to 3 mm) forms recrystallized polycrystalline aggregates. Plagioclase forms polygonal to rectangular aggregates with straight outer limits, composed of a mosaic of granoblastic plagioclase interspersed with interstitial muscovite flakes (both ~0.1 mm). Subhedral K-feldspar phenocrysts (up to 3 cm) include crystals of biotite, and recrystallized quartz and plagioclase. K-feldspar is commonly surrounded by a rim of myrmekite. Biotite is present in two textural positions. Red-brown biotite (biotite 1) forms large thick flakes (up to 3 mm) and is locally surrounded by thin coronae of garnet (Fig. 3e). Pale green biotite (biotite 2, up to 0.2 mm) is present in decussate subrectangular aggregates (up to 5 mm in size) with muscovite, garnet, kyanite, ±dravite, ±plagioclase, ±chlorite, and ±hematite. These clusters are interpreted as pseudomorphs after cordierite (Fig. 3f). In places, rutile (0.1 mm) builds up sub-rectangular aggregates (up to 0.5 mm) interpreted as pseudomorphs after ilmenite. Monazite, apatite, and zircon are found as accessory minerals.

Outer undeformed porphyritic facies

Sample LV2A (Fig. 3b) is a coarse-grained (2–10 mm) porphyritic granite mainly composed of quartz, plagioclase, porphyritic K-feldspar (up to 15 cm), and biotite. It bears some resemblance with the undeformed samples from the UGU (LV3, LV23), described above. Macroscopically, this sample appears isotropic, but various deformation and recrystallization features can be observed in thin section. K-feldspar forms large subhedral crystals with undulose extinction, locally cut by fractures filled with fine-grained quartz. Plagioclase forms subhedral crystals (up to 10 mm) that are generally partly altered to a mixture of tiny crystals of muscovite. Quartz is present as remnants of large anhedral crystals (up to 10 mm) with undulose extinction systematically surrounded by a mosaic of recrystallized grains with irregular grain boundaries. Large thick red-brown biotite (biotite 1, up to 5 mm) displays undulose extinction, and is in general affected by numerous kink-bands and locally surrounded by fine-grained symplectites containing quartz, rutile and muscovite (Fig. 3g). It is interpreted as a primary magmatic phase. Smaller light green to pale brown biotite flakes (biotite 2, up to 0.3 mm), interpreted as secondary, are present in sub-rectangular cm-sized decussate aggregates with muscovite (0.05-2 mm), and locally garnet, quartz and plagioclase (Fig. 3h). These aggregates may represent pseudomorphs after another "primary" mineral, possibly cordierite. Rutile (~0.1 mm) forms polycrystalline sub-rectangular to polygonal aggregates (up to 1 mm), interpreted as pseudomorphs after ilmenite. Monazite, zircon, and apatite are also present.

Outer augen orthogneiss (Pinet orthogneiss)

The rock (samples LV29 and LV2B, Fig. 3c) is a well-foliated felsic augen orthogneiss containing porphyroclasts (up to several cm) of K-feldspar and plagioclase. It represents the most common facies of the Pinet-type granitoids. The foliation is defined by alternating layers, up to 2 mm thick, dominated by either quartz, feldspar or phyllosilicates (biotite, muscovite and chlorite) and by the alignment of the latter (Fig. 3i). The foliation wraps augen composed of subhedral relics of K-feldspar or plagioclase (up to 3 cm), commonly partly recrystallized in strain shadows. The porphyroclasts are locally broken with quartz and chlorite crystallizing in the fractures. Biotite is strongly chloritized and chlorite in the foliation is interspersed by numerous tiny needles of rutile (sagenite) suggesting that it developed at the expense of biotite. Muscovite forms either large crystals (up to 1 mm) that can be kinked and wrapped by the foliation or small flakes (up to 0.1 mm) recrystallized in the foliation and commonly surrounding chloritized biotite. Allanite, titanite, apatite, zircon and rutile are also locally present.

Outer ultramylonitic facies

This sample (LV15) is a fine-grained ultramylonite with rare K-feldspar augen (Fig. 3d). The macroscopic fabric of the rock is defined by closely spaced (~5 mm) thin shear bands marked by very fine-grained (~0.01 mm) biotite, commonly associated with muscovite, quartz and feldspar. Thin (up to 0.3 mm) ribbons of strongly elongated quartz wrap small (up to 0.5 mm) crystals of K-feldspar and plagioclase. They are oblique to the shear bands and together with crystals of muscovite (up to 0.5 mm long) define a foliation. K-feldspar forms rare porphyroclasts (up to 1 cm), commonly rimmed by myrmekite and recrystallized in strain shadows (Fig. 3j). Chlorite is locally present in fractures in K-feldspar. Titanite, rutile, apatite, zircon and allanite are locally present.

Whole-rock compositions

These samples have the composition of a slightly peraluminous granite (A/CNK = 1.12–1.38; Fig. 4a, b; Table 1). They bear the general characteristics of the calc-alkaline series: (1) high abundances of Th and LREE (La_N ~ 145–180), (2) moderate fractionation of LREE versus HREE (La_N/Lu_N ~ 6.1–8.7) and a lack of important fractionation among the HREE (Fig. 4c), and (3) significant negative (Ta, Nb, Ti) and positive (Pb) anomalies (Fig. 4e). The chondrite-normalized REE patterns display the same trend for all the samples (including the same Eu anomaly range: $Eu_N = 0.022–0.032$) regardless of the deformation intensity (Fig. 4c). Taken together, the studied granites and granitic orthogneisses from the UGU and LGU have the same compositions, and deformation was not accompanied by a significant element mobility, with respect to the REE (Fig. 4c). The homogeneity of the whole-rock compositions of these different samples is also highlighted in the triangular Rb–Hf–Ta discrimination diagram (Harris et al. 1986; Fig. 4d). They fall into the "volcanic arc" domain, an expected result considering their calc-alkaline character (e.g., Ballèvre et al. 2012). Nevertheless, the tectonic setting can be either an active continental margin or the reworking of an older arc during a rifting event.

Rb–Sr and Sm–Nd radiogenic isotopes

Sr and Sm–Nd isotopic analyses for the 6 samples are listed in Table 2 and reported in Fig. 5. The ε_{Nd} and $^{87}Sr/^{86}Sr$ (I_{Sr}) values have been recalculated for an age of 470 Ma (see part 6). ε_{Nd} values are comprised between −5.66 and −5.29 for the six samples. I_{Sr} vary from 0.705635 to 0.714268. The T_{DM} (model age, calculated after Liew and Hofmann 1988) values vary from 1567 to 1596 Ma.

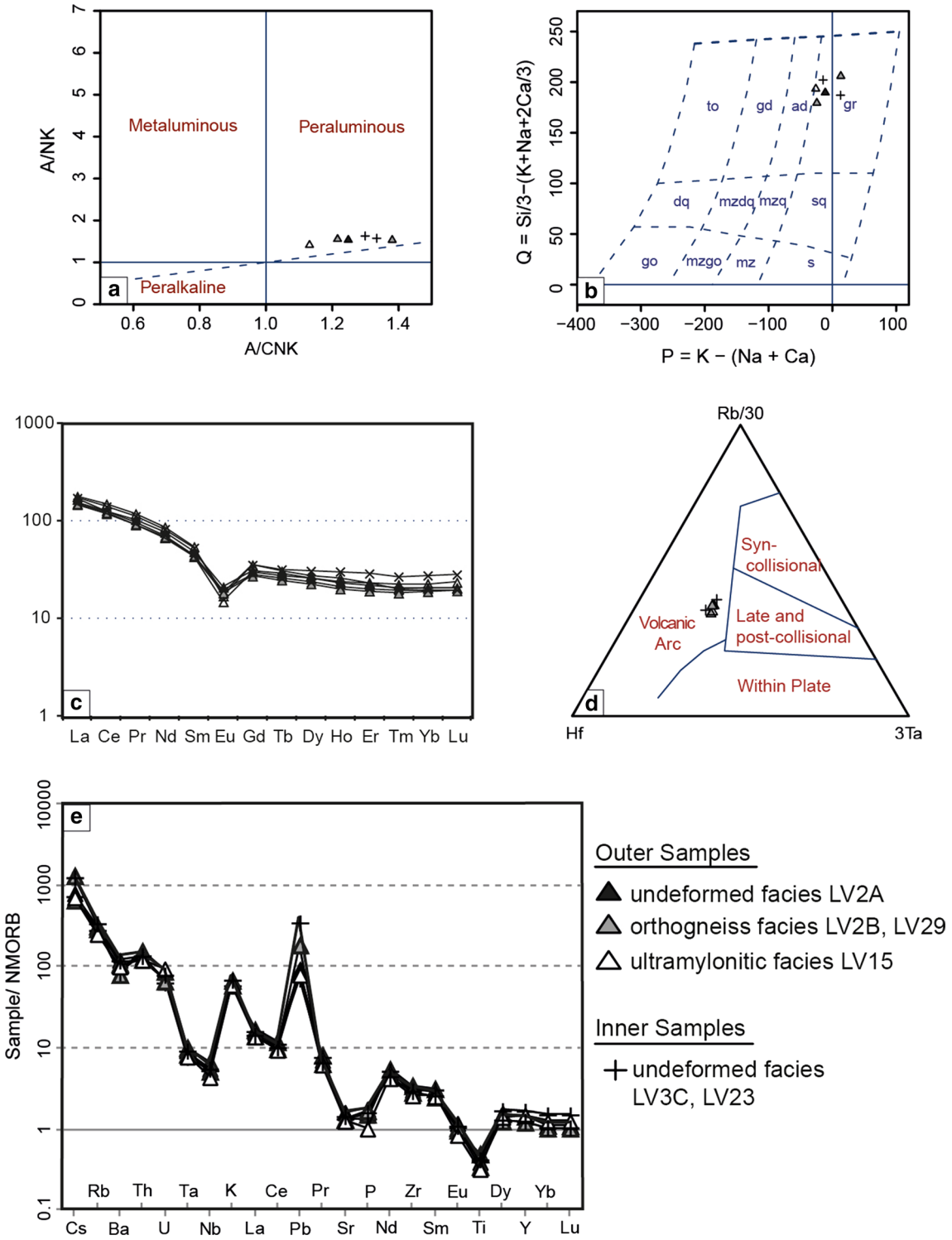

Fig. 4 Geochemical characteristics of the studied samples. *Triangles* and *crosses* correspond to outer (LV2A, LV2B, LV15, LV29) and inner (LV3, LV23) samples, respectively. **a** Shand (1943) diagram (A/CNK = Al_2O_3/(CaO + Na_2O + K_2O); A/NK = (Al_2O_3/Na_2O + K_2O)), **b** P-Q diagram after Debon and LeFort (1983), *gr* granite, *ad* adamellite, **c** chondrite-normalized REE distribution of all samples, values are normalized after Barrat et al. (2012), **d** ternary tectonic discrimination diagram from Harris et al. (1986), **e** N-MORB-normalized spider diagram after Sun and McDonough (1989)

Table 1 Whole-rock chemical compositions of the samples from outer (LV2A, LV2B, LV15, LV29) and inner (LV3, LV23) samples

Sample		Outer samples				Inner samples	
		LV 2A	LV 2B	LV 15	LV 29A	LV 23	LV 3C
SiO_2	wt %	70.43	71.24	71.31	68.63	70.30	68.65
Al_2O_3	wt %	14.59	14.39	13.64	14.36	14.34	14.61
Fe_2O_3	wt %	3.55	3.20	3.24	4.34	3.82	3.80
MnO	wt %	0.03	0.04	0.03	0.05	0.05	0.05
MgO	wt %	1.13	0.95	0.94	1.42	1.20	1.14
CaO	wt %	1.20	0.54	1.44	1.39	1.23	0.95
Na_2O	wt %	2.65	2.51	2.88	2.83	2.58	2.34
K_2O	wt %	4.73	4.90	4.34	4.29	4.25	4.98
TiO_2	wt %	0.51	0.44	0.42	0.63	0.52	0.55
P_2O5	wt %	0.21	0.20	0.12	0.18	0.16	0.19
LOI	wt %	1.70	2.05	1.29	1.68	1.57	1.73
FeO	wt %	2.31	1.86	2.48	X	2.68	2.62
As	ppm	6.14	10.76	2.43	7.70	3.49	13.87
Ba	ppm	760.70	685.30	635.00	503.80	535.20	748.60
Be	ppm	2.41	2.41	2.10	2.62	2.73	2.45
Bi	ppm	0.19	0.23	bdl	0.63	0.29	0.17
Cd	ppm	0.27	0.31	0.20	0.32	0.25	0.37
Ce	ppm	76.73	73.50	71.69	89.71	84.65	76.38
Co	ppm	6.01	6.12	5.02	8.45	6.32	6.05
Cr	ppm	49.31	56.71	39.03	67.31	41.15	48.47
Cs	ppm	5.57	4.60	4.98	9.16	5.13	8.72
Cu	ppm	14.46	12.77	7.11	26.71	16.35	11.96
Dy	ppm	6.58	5.78	6.52	7.08	7.83	6.01
Er	ppm	3.59	3.19	3.86	3.79	4.81	3.32
Eu	ppm	1.23	1.07	0.87	1.00	1.09	1.13
Ga	ppm	20.96	20.56	19.18	21.25	20.40	21.20
Gd	ppm	6.42	5.62	6.24	7.28	7.31	5.91
Ge	ppm	1.55	1.29	1.63	1.50	1.46	1.66
Hf	ppm	5.94	5.62	5.30	6.96	6.04	5.90
Ho	ppm	1.30	1.14	1.36	1.48	1.72	1.20
In	ppm	0.08	0.08	bdl	0.07	bdl	0.09
La	ppm	39.27	35.37	34.74	42.02	40.53	36.27
Lu	ppm	0.51	0.48	0.58	0.51	0.70	0.48
Mo	ppm	1.17	bdl	1.00	1.22	0.56	bdl
Nb	ppm	12.97	12.08	10.31	15.64	12.45	13.02
Nd	ppm	35.57	32.02	31.27	40.20	38.41	33.00
Ni	ppm	14.15	14.69	11.11	18.53	12.97	14.90
Pb	ppm	27.84	55.37	24.00	26.94	21.40	104.35
Pr	ppm	9.44	8.52	8.33	10.80	10.24	8.82
Rb	ppm	169.40	163.10	141.20	176.90	157.70	190.10
Sc	ppm	8.46	7.37	8.74	10.92	8.33	9.70
Sb	ppm	bdl	0.81	bdl	0.68	bdl	1.42
Sm	ppm	7.45	6.61	6.77	8.34	8.13	6.90
Sn	ppm	2.71	3.30	2.16	4.22	2.99	3.60
Sr	ppm	148.00	119.90	115.60	121.90	122.00	131.20
Ta	ppm	1.13	1.11	1.04	1.34	1.02	1.23
Tb	ppm	1.09	0.93	1.04	1.15	1.20	0.97
Th	ppm	15.76	14.69	14.62	18.64	16.48	16.21

Table 1 continued

Sample		Outer samples				Inner samples	
		LV 2A	LV 2B	LV 15	LV 29A	LV 23	LV 3C
Tm	ppm	0.54	0.48	0.58	0.53	0.71	0.51
U	ppm	3.18	3.12	4.44	4.11	3.00	3.73
V	ppm	45.00	37.76	31.54	51.61	41.75	48.41
W	ppm	1.62	4.13	0.95	1.22	1.25	1.72
Y	ppm	40.33	34.45	42.06	40.76	47.67	35.98
Yb	ppm	3.44	3.18	3.83	3.44	4.66	3.28
Zn	ppm	63.97	122.80	54.15	94.69	63.84	118.10
Zr	ppm	226.90	211.40	194.60	255.00	215.40	219.90
Total	%	100.74	100.45	99.65	99.79	100.00	98.97
A/NK		1.97	1.94	1.89	2.02	2.10	1.99
A/CNK		0.55	0.54	0.52	0.69	0.64	0.59

LOI loss on ignition, *A/NK* molar $Al_2O_3/(Na_2O + K_2O)$, *A/CNK* molar $Al_2O_3/(CaO + Na_2O + K_2O)$, *bdl* below detection limit, Fe_2O_3 corresponds to total Fe; FeO to Fe^{2+} only, analyzed by titration; *X* not analyzed

Table 2 Rb–Sr and Sm–Nd whole-rock data for the samples from outer (LV2A, LV2B, LV15, LV29) and inner (LV3, LV23) samples

Sample	Rb (ppm)	Sr (ppm)	$^{87}Rb/^{86}Sr$	$^{87}Sr/^{86}Sr$	±	I Sr_{470}	Sm (ppm)	Nd (ppm)	$^{147}Sm/^{144}Nd$	$^{143}Nd/^{144}Nd$	±	$\varepsilon_{Nd\,(470)}$	T_{DM} [a]
Outer samples													
LV 2A	169.40	133.9	3.67	0.733146	10	0.708563	6.9	35.1	0.118651	0.512110	4	−5.62	1.593
LV 2B	163.10	107.1	4.42	0.735226	10	0.705635	6.1	30.6	0.121020	0.512118	5	−5.61	1.592
LV 15	115.60	105.7	3.17	0.734002	10	0.712742	6.5	31.6	0.124813	0.512141	4	−5.38	1.575
LV 29A	176.90	117.2	4.38	0.736913	10	0.707572	8.1	42.0	0.116544	0.512117	5	−5.35	1.572
Inner samples													
LV 3C	141.20	118.2	3.47	0.737488	10	0.714268	6.4	32.6	0.118418	0.512107	5	−5.66	1.596
LV 23	157.70	117.9	3.88	0.733453	12	0.707455	7.5	38.7	0.116902	0.512122	4	−5.29	1.567

Rb concentrations have been obtained by ICP-MS, other concentrations by isotopic dilution

ε_{Nd} and $^{87}Sr/^{86}Sr$ are calculated with an age of 470 Ma

[a] $^{87}Rb/^{86}Sr$ ratios are calculated after Janoušek et al. (2015, p. 54, Eq. 5.4) and the two-stage T_{DM} model age after Liew and Hofmann (1988)

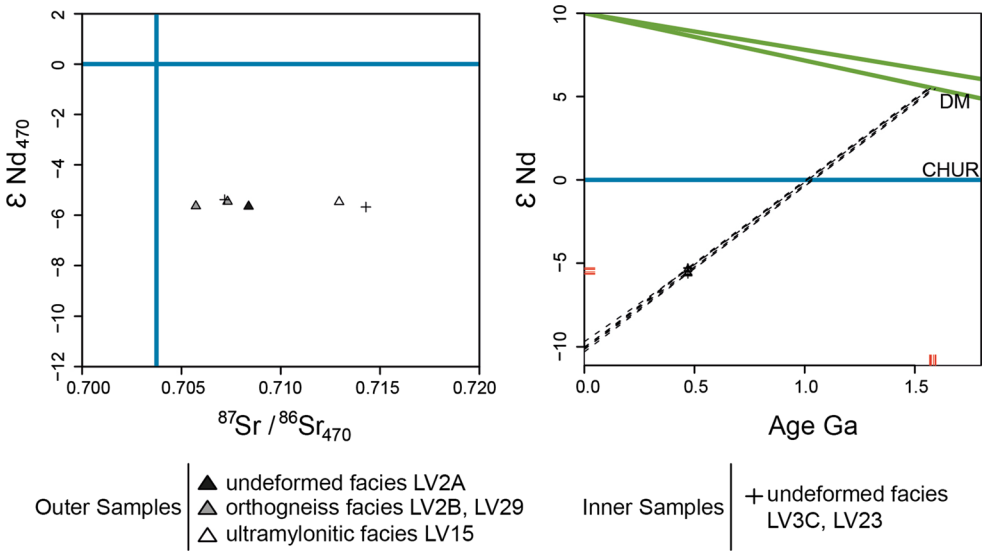

Fig. 5 **a** Sr and Nd isotope composition of the samples. ε_{Nd} and $^{87}Sr/^{86}Sr$ are calculated with an age of 470 Ma (see part 6). *Crosses* represent the undeformed samples outcropping in the inner part of the massif (LV3C, LV23) and *triangles* correspond to the samples from the outer part (Pinet orthogneiss s.s., LV2A, LV2B, LV29 and LV15). **b** Two-stage T_{DM} model age, calculated after Liew and Hofmann (1988). Marks on x- and y-axis correspond to the two-stage Nd model age and ε_{Nd} initial values, respectively. *CHUR* Chondritic Uniform Reservoir, *DM* Depleted Mantle

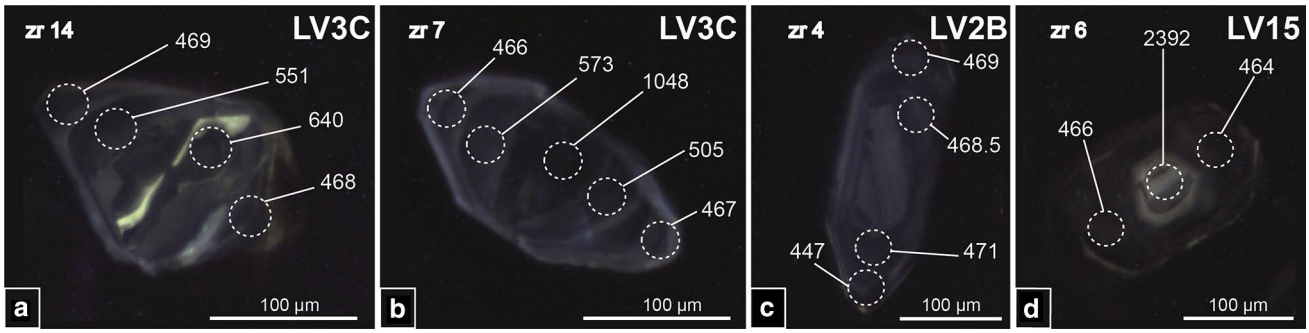

Fig. 6 Selected cathodoluminescence images of zircon crystals from samples LV3C (**a**, **b**), LV2B (**c**) and LV15 (**d**). *Dotted circles* show the location of the LA-ICP-MS analyses and their corresponding $^{238}U/^{206}Pb$ ages

The ε_{Nd} values display very little variation, as usually observed within the same pluton (e.g., Ballouard et al. 2015). In contrast, I_{Sr} values are more spread (Fig. 6). Rubidium and strontium are known to be mobile under metamorphism, deformation, or fluid alteration. Moreover, a large range of I_{Sr} can also reflect variable sedimentary sources involved in magma production. The range of values is then likely explained by the highly variable patterns of deformation that affected the different facies, by alteration, or by its sedimentary origin (see part 4—Whole-rock compositions). Finally, the samples yield the same model age range. Considering the large range of inherited zircon cores (see part 5—U–Th–Pb Dating) and the peraluminous character of the rocks (see part 4—Whole-rock compositions), reworking of multiple sedimentary sources is the most likely explanation for these old ages, and these T_{DM} should then be seen as a mean age of the sedimentary source rather than as an extraction age from the mantle.

U–Th–Pb dating

Zircon crystals were extracted from samples LV2A, LV2B, LV15, and LV3C, located on both sides of the LAC (Fig. 2). All crystals were translucent and colorless, with heterogeneous shapes from rounded to euhedral, ranging from 100 to 400 µm in size. Most of the grains have inherited cores surrounded by magmatic rims (Fig. 6a, b, d). Locally, inherited cores are surrounded by a primary zonation, and by a magmatic rim, as revealed by cathodoluminescence imaging (Fig. 6b). Numerous purely magmatic zircon crystals are also found (Fig. 6c).

Most of the inherited cores show high degrees of discordance (see Supplementary Table 2), and it is therefore impossible to discuss them in terms of provenance. All data that are more than 90 % concordant (and less than 110 %) are plotted in a kernel density estimates diagram (Fig. 7e). Apart from the magmatic rim that will be discussed later, a first group of inherited cores provides apparent ages between 500 and 760 Ma. A second group is bracketed around 1 Ga, while the remaining data yield apparent ages between 1700 and 3200 Ma.

Inner undeformed porphyritic facies

Sixty-six analyses were performed out of 18 different zircon grains from sample LV3C (Supplementary Table 2). Apart from the inherited core discussed above, 33 analyses performed on magmatic zircon crystals without inherited core and/or on crystal rims were plot in concordant to discordant position (Fig. 7a) due to various degrees of Pb loss and/or the presence of common Pb. Nevertheless, all these analyses have very consistent $^{206}Pb/^{238}U$ dates and provide a lower intercept date of 466.6 ± 3.3 Ma (MSWD = 0.14). The five most concordant analyses yield a concordia date of 467.8 ± 2.3 Ma (MSWD = 0.3). It has to be noticed that one single analysis performed on a rim (Supplementary Table 2, 18b) plots in an apparently concordant position at 414.1 ± 4.7 Ma. But another spot (18a) realized on the same rim from the same grain yields a concordant date of 468.7 ± 5.3 Ma. We conclude therefore that the younger date is linked to a slight Pb loss.

Outer undeformed porphyritic facies

Sixty-nine analyses were performed out of 38 zircon grains in sample LV2A (Supplementary Table 2). All magmatic rims yield $^{206}Pb/^{238}U$ dates bracketed around 470 Ma (Fig. 7b, e) and allow to calculate a lower intercept date of 468.2 ± 2.7 Ma (MSWD = 0.7; $N = 34$). The 10 most concordant data (Fig. 7b) yield a concordia date of 469.8 ± 1.6 Ma (MSWD = 0.56), while the remaining analyses are slightly discordant due to the presence of a small amount of common Pb and/or Pb loss.

Outer orthogneissic facies (Pinet orthogneiss)

In the augen orthogneiss LV2B, 16 zircon grains were analyzed (Supplementary Table 2; Fig. 7c). Most of the 30 analyses display discordant dates. The four youngest concordant analyses allow to calculate a concordia date of 469.8 ± 2.7 Ma (MSWD = 0.26). Six concordant to discordant analyses allow to calculate a lower intercept date of 470.5 ± 5.2 Ma (MSWD = 0.30), the same within error as the calculated concordia date. Eight of the remaining analyses are discordant, ranging from 420 to 480 Ma, and can be explained by variable lead loss and common lead enrichment. Twelve rim analyses range from 496 to 765 Ma.

Outer ultramylonitic facies

Eighty-two analyses on 30 different zircon crystals were performed for sample LV15. A group of 31 concordant to discordant analyses (common Pb and/or Pb loss) allows to calculate a lower intercept date of 465.6 ± 2.6 Ma (MSWD = 0.66). An equivalent (within the error) concordia date was calculated with the 5 concordant spots, yielding a date of 468 ± 1.3 Ma (MSWD = 0.98) (Fig. 7d). Three analyses display younger dates ranging from 427 to 311 Ma ($^{206}Pb/^{238}U$), which can be explained by a combination of lead loss and common lead enrichment.

Inherited cores from all the four samples range from 500 Ma to 3 Ga, show various lead loss, and display concordant to discordant dates. Three populations can be distinguished in the inherited cores and primary zonation: (1) few Precambrian dates, from ca. 3.3–1 Ga, in discordant position, (2) Precambrian dates from ca 770 to 550 Ma, in concordant to sub-concordant position, and (3) few Cambrian dates ranging from 550 to 500 Ma (Fig. 7e). All the rims of the zircon grains with inherited cores recorded an Ordovician event at ca. 470 Ma. Besides, all zircon crystals without inherited cores yield equivalent ages (within error) at ca. 470 Ma, obtained by lower intercepts in Tera–Wasserburg diagrams and by concordia dates (Fig. 7a–d). In conclusion, all analyzed samples, regardless of their position with respect to the LAC and the deformation intensity, yield the same Ordovician age of ca. 470 Ma, interpreted as the age of the emplacement of the granitic protoliths.

Discussion

The Pinet-type granitoids: Ordovician intrusions

An Ordovician event around 470 Ma is recorded by all the granitoid samples, independently from the facies from which they were extracted, the presence or absence of inherited cores in the studied zircon crystals, or the deformation intensity. As both undeformed and ultramylonitic samples provide the same age, the U–Pb chronometer has not been affected by deformation. Previous dating of the Pinet orthogneiss (ca. 360 Ma, Pin 1981) was performed on zircon fractions, meaning that a large amount of grains has been dissolved and then dated. Pin noticed the presence of inherited cores in some of the crystals, but, although he tried to avoid them during the picking, the data obtained plot systematically in a discordant position with evidence for mixing between a magmatic age and different apparent inherited ages. In addition, Pb loss is evidenced by the lack of a simple linear array and the proposed age of ca. 360 Ma (lower intercept) is mostly constrained by the analysis of one fraction of apatite crystals that plots also in a discordant position. Consequently, the proposed ca. 360 Ma age for the emplacement of the protolith of the Pinet orthogneiss must be discarded and the Pinet orthogneiss cannot be syn-kinematic with respect to the Late Devonian-Early Carboniferous thrusting events as previously suggested (Burg and Teyssier 1983; Burg 1987; Dutruge and Burg 1997; Duguet and Faure 2004). Considering the gradual transition observed by Nicollet (1978) between the Pinet orthogneiss and the metarhyolite from the PAU, the Cambrian Rb/Sr age (Delbos et al. 1964) of the latter should also be reconsidered.

Tectonic and geodynamic implications for the Lévézou massif

Both the inner and the outer granitoids/orthogneisses display the same age, the same textures, the same chemical composition, the same REE spectrum, the same radiogenic isotope values, and the same T_{DM} age. Consequently, all these granitoids originated from the same magmatic source. The Pinet-type granitoids therefore belong to the Ordovician magmatic event that is well documented at the scale of the Variscan orogen (see "Introduction"). The precise geodynamic context of this event (i.e., extended continental margin, back-arc basin) is debated, although most interpretations consider that magmatism resulted from extreme lithosphere thinning (Gondwana breakup, opening of the Rheic Ocean) during Ordovician times (e.g., Lardeaux 2014). The 470 Ma age obtained on the granitoids of the Lévézou massif is markedly older than the 460–455 Ma age obtained on the orthogneisses from the Montagne Noire ~ 50 km farther to the south, suggesting a migration of the magmatic source during the Ordovician extension.

The occurrence of similar granitoids of the same age on each side of the LAC suggests two end-member interpretations. (1) The UGU and LGU in the Lévézou massif were originally two continental margins of an ocean or a back-arc basin during Ordovician times. The stacking of the UGU, LAC and LGU occurred during the Variscan tectonics. (2)

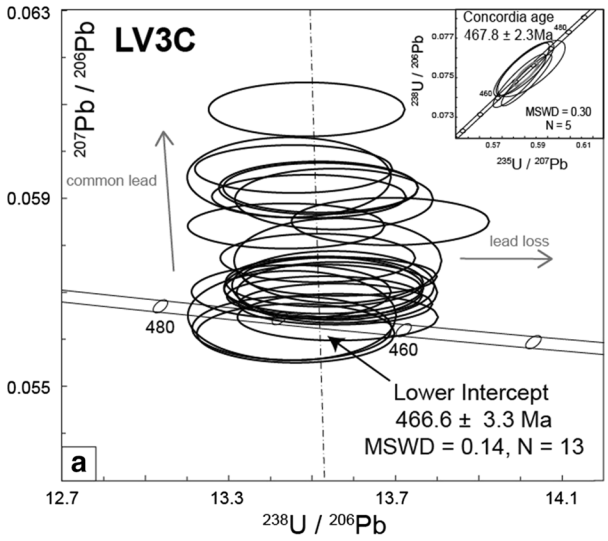
LV3C
Concordia age
467.8 ± 2.3Ma
MSWD = 0.30
N = 5
common lead
lead loss
480
460
Lower Intercept
466.6 ± 3.3 Ma
MSWD = 0.14, N = 13
a
0.063
0.059
0.055
12.7
13.3
13.7
14.1
207Pb / 206Pb
238U / 206Pb
235U / 207Pb
238U / 206Pb

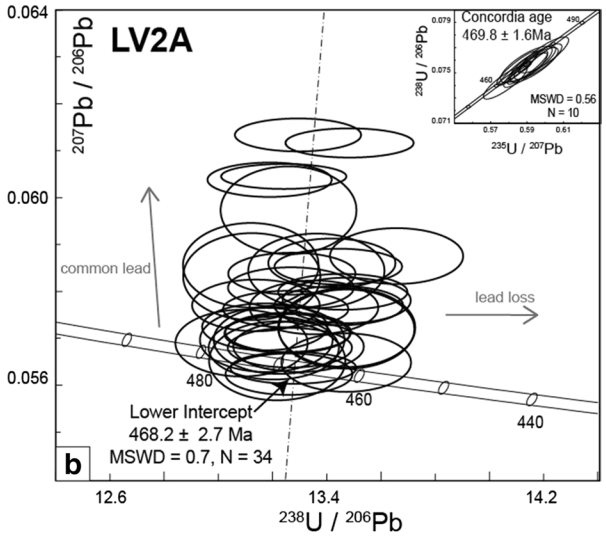
LV2A
Concordia age
469.8 ± 1.6Ma
MSWD = 0.56
N = 10
common lead
lead loss
480
460
440
Lower Intercept
468.2 ± 2.7 Ma
MSWD = 0.7, N = 34
b
0.064
0.060
0.056
12.6
13.4
14.2
207Pb / 206Pb
238U / 206Pb
235U / 207Pb

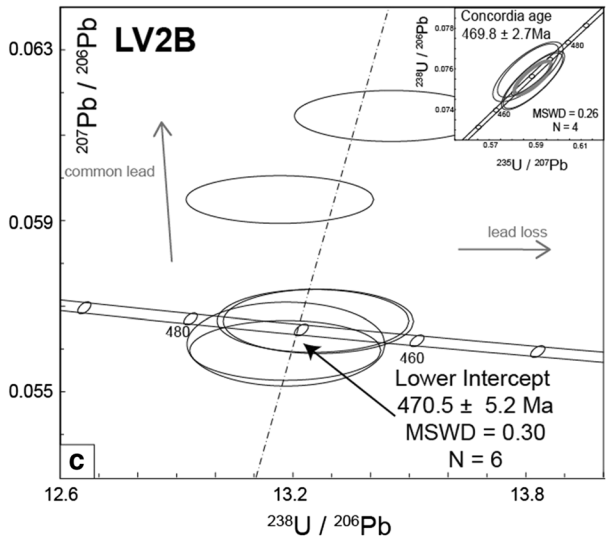
LV2B
Concordia age
469.8 ± 2.7Ma
MSWD = 0.26
N = 4
common lead
lead loss
480
460
Lower Intercept
470.5 ± 5.2 Ma
MSWD = 0.30
N = 6
c
0.063
0.059
0.055
12.6
13.2
13.8
207Pb / 206Pb
238U / 206Pb
235U / 207Pb

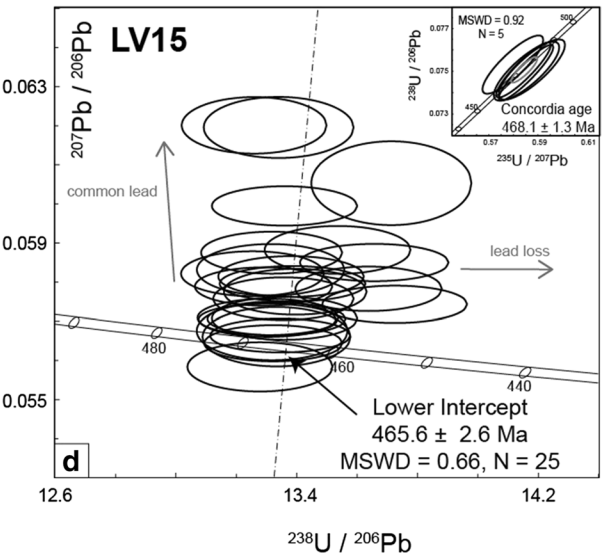
LV15
MSWD = 0.92
N = 5
Concordia age
468.1 ± 1.3 Ma
common lead
lead loss
480
460
440
Lower Intercept
465.6 ± 2.6 Ma
MSWD = 0.66, N = 25
d
0.063
0.059
0.055
12.6
13.4
14.2
207Pb / 206Pb
238U / 206Pb
235U / 207Pb
238U / 206Pb

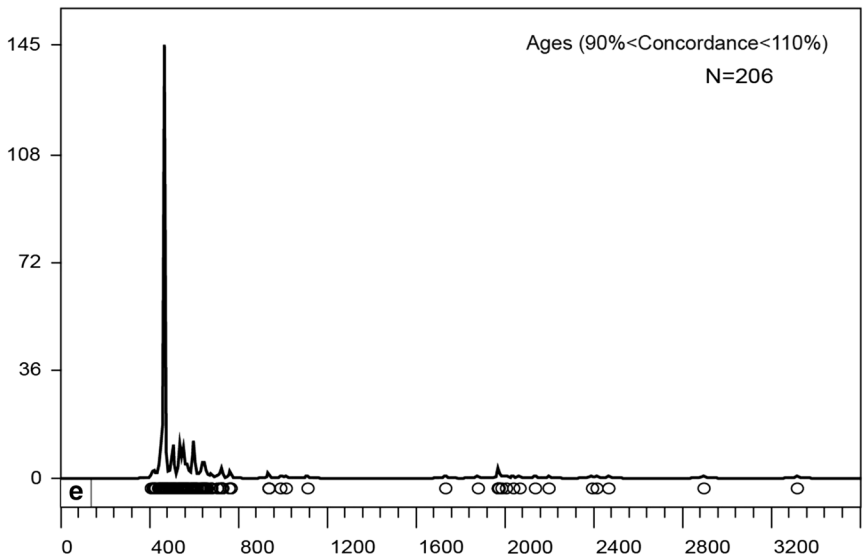
Ages (90%<Concordance<110%)
N=206
145
108
72
36
0
e
0
400
800
1200
1600
2000
2400
2800
3200

◂**Fig. 7** Tera–Wasserburg ($^{207}Pb/^{206}Pb$ vs $^{238}U/^{206}Pb$) and Wetherill ($^{238}U/^{206}Pb$ vs $^{235}U/^{207}Pb$) concordia diagrams displaying Ordovician analyses made on zircon from samples **a** LV3C, **b** LV2A, **c** LV2B, **d** LV15. **e** kernel diagram (Vermeesch 2012) on the U/Pb data from this study (90–110 % concordance only)

The UGU and LGU were originally a single Ordovician unit (a continental margin or an arc) and the LAC represented the adjacent oceanic crust that was under- or overthrusted during Early Variscan tectonics, resulting in a major tectonic contact. The occurrence of this single unit on each side of the LAC requires either isoclinal nappe refolding as previously proposed (Burg and Teyssier 1983) or tectonic duplication by superimposed shearing events during ongoing Variscan tectonics. The identical isotopic signature of the granitoids on each side of the LAC favors the single-unit hypothesis (2). However, in order to settle the tectonic interpretation, new quantitative PT and age data on other metamorphic rocks are required. This work, dedicated to comparing the metamorphic evolution of the orthogneisses and adjacent rocks on both sides of the LAC, is in progress.

Conclusion

New U–Pb ages of ca. 470 Ma of the granitoids from the Lévézou massif in the southern Massif Central reveal that these intrusions belong to the major magmatic event that developed throughout the European Variscan belt during the Early-Middle Ordovician extensional tectonics. As a consequence, the Pinet-type orthogneisses are not syn-tectonic intrusions emplaced during the Late Devonian-Early Carboniferous Variscan collision, as previously thought. The similar ages, chemical compositions, and isotopic signatures of these granitoids in the Lévézou massif as a whole strongly suggest that the Lower and Upper gneissic units (UGU and LGU), on each side of the leptyno-amphibolitic complex (LAC), were originally a single unit, tectonically duplicated either by isoclinal folding or thrusting during the Variscan tectonics.

Acknowledgments We sincerely thank X. Le Coz and Y. Lepagnot for the sample preparation, J. Langlade for the assistance with microprobe analysis, and D. Vilbert for the Sm/Nd and Sr isotopic analysis. V. Janoušek and P. Boulvais are thanked for helpful discussions about the whole-rock and isotopic geochemistry. Constructive reviews of P. Jeřábek and J.M. Lardeaux helped to improve the manuscript.

References

Abati J, Dunning GR, Arenas R, García FD, Cuadra PG, Catalán JM, Andonaegui P (1999) Early Ordovician orogenic event in Galicia (NW Spain): evidence from U–Pb ages in the uppermost unit of the Ordenes Complex. Earth and Planetary Science Letters 165:213–228

Ballèvre M, Bosse V, Ducassou C, Pitra P (2009) Palaeozoic history of the Armorican Massif: models for the tectonic evolution of the suture zones. C R Geosci 341:174–201

Ballèvre M, Fourcade S, Capdevila R, Peucat JJ, Cocherie A, Fanning CM (2012) Geochronology and geochemistry of Ordovician felsic volcanism in the Southern Armorican Massif (Variscan belt, France): implications for the breakup of Gondwana. Gondwana Res 21:1019–1036

Ballèvre M, Martínez Catalán JR, López-Carmona A, Pitra P, Abati J, Díez Fernández R, Ducassou C, Arenas R, Bosse V, Castiñeiras P, Fernández-Suárez J, Gómez Barreiro J, Paquette J-L, Peucat J-J, Poujol M, Ruffet G, Sánchez Martínez S (2014) Correlation of the nappe stack in the Ibero-Armorican arc across the Bay of Biscay: a joint French-Spanish project. In: Schulmann K, Martínez Catalán JR, Lardeaux J-M, Janoušek V, Oggiano G (eds) The Variscan orogeny: extent, timescale and the formation of the European Crust. Geol Soc Lond 405:77–113

Ballouard C, Boulvais P, Poujol M, Gapais D, Yamato P, Tartèse R, Cuney M (2015) Tectonic record, magmatic history and hydrothermal alteration in the Hercynian Guérande leucogranite, Armorican Massif, France. Lithos 220–223:1–22

Bard JP, Burg JP, Matte P, Ribeiro A (1980) La Chaîne Hercynienne d'Europe Occidentale en termes de tectonique des plaques. In: International geological congress, 26th mémber BRGM, Paris, vol 108, pp 233–246

Barrat JA, Zanda B, Moynier F, Bollinger C, Liorzou C, Bayon G (2012) Geochemistry of CI chondrites: major and trace elements, and Cu and Zn Isotopes. Geochim Cosmochim Acta 83:79–92

Berger J, Féménias O, Ohnenstetter D, Bruguier O, Plissart G, Mercier JC, Demaiffe D (2010) New occurrence of UHP eclogites in Limousin (French Massif Central): age, tectonic setting and fluid–rock interactions. Lithos 118:365–382

Briand B, Piboule M, Bouchardon JL (1988) Diversité géochimique des métabasites des groupes leptyno-amphiboliques du Rouergue et de Marvejols (Massif central). Origine et implications. Bull Soc Géol France 8:489–498

Burg JP (1987) Regional shear variation in relation to diapirism and folding. J Struct Geol 9:925–934

Burg JP, Matte P (1978) A cross section through the French Massif Central and the scope of its Variscan evolution. Z Dtsch Geol Ges 129:429–440

Burg JP, Teyssier C (1983) Contribution à l'étude tectonique et microtectonique des séries cristallophyliennes du Rouergue oriental: la déformation des laccolites syntectoniques, type Pinet. Géol France 1:3–30

Burg JP, Delor C, Leyreloup A (1986) Le massif du Lévezou et les séries adjacentes du Rouergue oriental. Nouvelles données pétrographiques et structurales. Géol France 3:229–272

Burg JP, Van Den Driessche J, Brun JP (1994) Syn-to post-thickening extension in the Variscan Belt of Western Europe: modes and structural consequences. Géol France 3:33–51

Carignan J, Hild P, Mevelle G, Morel J, Yeghicheyan D (2001) Routine analyses of trace elements in geological samples using flow injection and low pressure on-line liquid chromatography coupled to ICP-MS: a study of geochemical reference materials BR, DR-N, UB-N, AN-G and GH. Geostandards Newslett 25:187–198

Collomb P (1970) Etude géologique du Rouergue cristallin. Mém. Expl. Serv. Carte Géological, Paris

Crowley QG, Floyd PA, Winchester JA, Franke W, Holland JG (2000) Early Palaeozoic rift-related magmatism in Variscan Europe: fragmentation of the Armorican Terrane Assemblage. Terra Nova 12(4):171–180

Debon F, LeFort P (1983) A chemical–mineralogical classification of common plutonic rocks and associations. Trans R Soc Edinburgh: Earth Sci 73:135–149

Del Greco K, Johnston ST, Shaw J (2016) Tectonic setting of the North Gondwana margin during the Early Ordovician: a comparison of the Ollo de Sapo and Famatina magmatic events. Tectonophysics 681:73–84

Delbos L, Lasserre M, Roques M (1964) Géochronologie et rétromorphose dans la série cristallophyllienne du Rouergue (Massif central français). Sci Terre 10:329–342

Delor C, Leyreloup A, Burg JP (1985) Nouveaux arguments pétrologiques enfaveur de l'allochtonie du Lévézou (Massif Central français): les enclaves basiques des granites calco-alcalins et les métacornéennes associées. C R Acad Sci Paris 301:1037–1042

Delor C, Burg JP, Leyreloup A, Teyssier C (1989) Carte géol France (1/50000), feuille Salles Curan(908). BRGM, Orléans

Dewey JF, Burke KCA (1973) Tibetan, Variscan, and precambrian basement reactivation: products of continental collision. J Geol 81:683–692

Ducrot J, Lancelot JR, Marchand J (1983) Datation U–Pb sur zircons de l'éclogite de la Borie (Haut-Allier, France) et conséquences sur l'évolution anté-hercynienne de l'Europe occidentale. Earth Planet Sci Lett 18:97–113

Duguet M, Faure M (2004) Successive shearing tectonics during the hercynian collisional evolution of the southwestern French Massif Central. Bull Soc Geol France 175:49–59

Dutruge G, Burg JP (1997) Strain localisation in an orthogneiss laccolith (the Pinet massif, Aveyron, southern France). Tectonophysics 280:47–60

Forestier FH (1961) Métamorphisme hercynien et antéhercynien dans le bassin du haut-Allier (Massif Central français), PhD Thesis, Clermont-Ferrand University

Forestier FH, Lasnier B, Leyreloup A, Marchand J (1973) Vues nouvelles sur la catazone dans le Massif Central français et le Massif Armoricain de l'affleurement au Moho. Bull Soc Géol France 15:562–578

Franke W (2006) The Variscan orogen in Central Europe: construction and collapse. Memoirs Geol Soc London 32:333–343

Guérangé-Lozes J, Burg JP, Vinchon C, Alabouvette B, Defaut B, Astruc JG, Galharague J, Leyreloup A, Michard AG, Perrin C, Servelle S (1995) Carte géol France (1/50000), feuille Requista(934). BRGM, Orléans

Harris NB, Pearce JA, Tindle AG (1986) Geochemical characteristics of collision-zone magmatism. Geol Soc Lond Spec Publ 19:67–81

Helbing H, Tiepolo M (2005) Age determination of Ordovician magmatism in NE Sardinia and its bearing on Variscan basement evolution. J Geol Soc 162:689–700

Jackson SE, Pearson NJ, Griffin WL, Belousova EA (2004) The application of laser ablation-inductively coupled plasma-mass spectrometry to in situ U–Pb zircon geochronology. Chem Geol 211:47–69

Janousek V, Moyen JF, Martin H, Erban V, Farrow C (2015) Geochemical modelling of igneous processes–principles and recipes in R Language: bringing the Power of R to a Geochemical Community. Springer, Berlin, 347 p

Janoušek V, Farrow CM, Erban V (2006) Interpretation of whole-rock geochemical data in igneous geochemistry: introducing Geochemical Data Toolkit (GCDkit). J Petrol 47:1255–1259

Lafon JM (1984) La granodiorite de Caplongue, nouveau témoin d'un magmatisme cambrien dans le Rouergue oriental. C R Acad Sci Paris 298:595–600

Lardeaux JM (2014) Deciphering orogeny: a metamorphic perspective Examples from European Alpine and Variscan belts Part II: Variscan metamorphism in the French Massif Central—a review. Bull Soc Géol France 185:281–310

Lasnier B (1968) Découverte de roches éclogitiques dans le groupe leptyno-amphibolique des monts du Lyonnais (Massif central français). Bull Soc Géol France 7:179–185

Ledru P, Lardeaux JM, Santallier D, Autran A, Quenardel JM, Floc'h JP, Lerouge G, Maillet N, Marchand J, Ploquin A (1989) Où sont les nappes dans le Massif central français? Bull Soc Géol Fr 3:605–618

Liew TC, Hofmann AW (1988) Precambrian crustal components, plutonic associations, plate environment of the Hercynian Fold Belt of central Europe: indications from a Nd and Sr isotopic study. Contrib Miner Petrol 98:129–138

Linnemann U, McNaughton NJ, Romer RL, Gehmlich M, Drost K, Tonk C (2004) West African provenance for Saxo-Thuringia (Bohemian Massif): Did Armorica ever leave pre-Pangean Gondwana?—U/Pb-SHRIMP zircon evidence and the Nd-isotopic record. Int J Earth Sci 93(5):683–705

Ludwig KR (2012) User's manual for a geochronological toolkit for Microsoft Excel. Berkeley Geochronological Cent, 75

Martínez Catalán JR, Arenas R, Abati J, Sánchez Martínez S, Díaz García F, Fernández-Suárez J, González Cuadra P, Castiñeiras P, Gómez Barreiro J, Díez Montes A, Gónzalez Clavijo E, Pascual FJR, Andonaegui P, Jeffries TE, Alcock JE, Díez Fernández R, López Carmona A (2009) A rootless suture and the loss of the roots of a mountain chain: the Variscan belt of NW Iberia. CR Geosci 341:114–126

Matte P (1986) Tectonics and plate tectonics model for the Variscan belt of Europe. Tectonophysics 126:329–374

Matte P (1991) Accretionary history of the Variscan belt in western Europe. Tectonophysics 196:309–337

Matte P (2001) The Variscan collage and orogeny (480–290 Ma) and the tectonic definition of the Armorica microplate: a review. Terra Nova 13(2):122–128

Matte P, Burg JP (1981) Sutures, thrusts and nappes in the Variscan arc of Western Europe: plate tectonic implication. In: McClay K, Price NJ (eds) Thrust and Nappe Tectonics. Geol Soc Lond Spec Publ 8:353–357

Montero P, Talavera C, Bea F, Lodeiro FG, Whitehouse MJ (2009) Zircon Geochronology of the Ollo de Sapo formation and the age of the Cambro-Ordovician Rifting in Iberia. J Geol 117(2):174–191

Nicollet C (1978) Pétrologie et tectonique des terrains cristallins antépermiens du versant sud du dôme du Lévezou (Rouergue, Massif central). Bull BRGM 3:225–263

Paquette JL, Monchoux P, Couturier M (1995) Geochemical and isotopic study of a norite-eclogite transition in the European Variscan Belt: implications for U–Pb zircon systematics in metabasic rocks. Geochim Cosmochim Acta 59:1611–1622

Paquette JL, Piro JL, Devidal JL, Bosse V, Didier A, Sanac S, Abdelnour Y (2014) Sensitivity enhancement in LA-ICP-MS by N2 addition to carrier gas: application to radiometric dating of U–Th-bearing minerals. Agilent ICP-MS J 58:1–5

Piboule M (1979) L'origine des amphibolites: approche géochimique et mathématique. Application aux amphibolites du Massif central français. Thèse d'Etat, Lyon I University

Pin C (1979) Géochronologie U–Pb et microtectonique des séries métamorphiques anté-stéphaniennes de l'Aubrac et de la région de Marvejols (Massif central). PhD Thesis, Montpellier University

Pin C (1981) Old inherited zircons in two synkinematic variscan granitoids: the «granite du Pinet» and the «orthogneiss de Marvejols» (southern French Massif central). N J Miner Abh 142:27–48

Pin C (1990) Variscan oceans: ages, origins and geodynamic implications inferred from geochemical and radiometric data. Tectonophysics 177:215–227

Pin C, Lancelot J (1982) U–Pb dating of an early Paleozoïc bimodal magmatism in the French Massif central and its further metamorphic evolution. Contrib Mineral Petrol 79:1–12

Pin C, Marini F (1993) Early Ordovician continental break-up in Variscan Europe: Nd–Sr isotope and trace element evidence from

bimodal igneous associations of the Southern Massif Central, France. Lithos 29(3):177–196

Pin C, Piboule M (1988) Upper Devonian U–Pb zircon age of the calc-alkaline series in the Levezou mafic belt, Rouergue (Massif Central, France). A composite leptyno-amphibolitic association. Bull Soc Géol Fr 4:261–265

Pin C, Vielzeuf D (1983) Granulites and related rocks in Variscan median Europe: a dualistic interpretation. Tectonophysics 93:47–74

Pitra P, Poujol M, Van Den Driessche J, Poilvet JC, Paquette JL (2012) Early Permian extensional shearing of an Ordovician granite: the Saint-Eutrope "C/S-like" orthogneiss (Montagne Noire, French Massif Central). Comptes Rendus Géoscience 344:377–384

Ribeiro A, Munhá J, Dias R, Mateus A, Pereira E, Ribeiro L, Fonseca P, Araújo A, Oliveira T, Romão J, Chaminé H, Coke C, Pedro J (2007) Geodynamic evolution of the SW Europe Variscides. Tectonics 26:1–24 TC6009

Roger F, Respaut JP, Brunel M, Matte P, Paquette JL (2004) U–Pb dating of Augen orthogneisses from the axial zone of the Montague Noire (Southern of Massif Central): new witness of Ordovician magmatism into the Variscan Belt. Comptes Rendus Géoscience 336:19–28

Sánchez-García T, Bellido F, Quesada C (2003) Geodynamic setting and geochemical signatures of Cambrian-Ordovician rift-related igneous rocks (Ossa-Morena Zone, SW Iberia). Tectonophysics 365(1–4):233–255

Sánchez-García T, Quesada C, Bellido F, Dunning GR, González del Tánago J (2008) Two-step magma flooding of the upper crust during rifting: the Early Paleozoic of the Ossa Morena Zone (SW Iberia). Tectonophysics 461(1–4):72–90

Santallier D, Briand B, Menot RP, Piboule M (1988) Les complexes leptyno-amphiboliques (C.L.A.); revue critique et suggestions pour un meilleur emploi de ce terme. Bull Soc Géol Fr 4:3–12

Schulmann K, Catalán JR, Lardeaux JM, Janoušek V, Oggiano G (2014) The Variscan orogeny: extent, timescale and the formation of the European crust. Geol Soc Lond Spec Publ 405:1–6

Shand SJ (1943) Eruptive rocks. Their genesis, composition, classification, and their relation to ore-deposits with a chapter on meteorite. Wiley, New York

Solá AR, Pereira MF, Williams IS, Ribeiro ML, Neiva AM, Montero P, Bea F, Zinger T (2008) New insights from U–Pb zircon dating of Early Ordovician magmatism on the northern Gondwana margin: the Urra Formation (SW Iberian Massif, Portugal). Tectonophysics 461:114–129

Sun SS, McDonough WF (1989) Chemical and isotopic systematics of oceanic basalts: implications for mantle composition and processes. Geol Soc Lond Spec Publ 42:313–345

Talavera C, Montero P, Bea F, González Lodeiro F, Whitehouse M (2013) U–Pb Zircon geochronology of the Cambro-Ordovician metagranites and metavolcanic rocks of central and NW Iberia. Int J Earth Sci 102:1–23

Van Achterbergh E, Ryan CG, Jackson SE, Griffin WL (2001) Data reduction software for LA-ICP-MS: appendix. In: Sylvester PJ (ed) Laser Ablation-ICP-mass spectrometry in the earth sciences: principles and applications. In Mineralog Assoc Canada (MAC) Short Courses Series, Ottawa, vol 29, pp 239–243

Vermeesch P (2012) On the visualisation of detrital age distributions. Chem Geol 312–313:190–194

Wiedenbeck M, Allé P, Corfu F, Griffin WL, Meier M, Oberli F, von Quadt A, Roddick JC, Spiegel W (1995) Three natural zircon standards for U–Th–Pb, Lu–Hf, trace element and REE analyses. Geostand Newsl 19:1–23

Young TP (1990) Ordovician sedimentary facies and faunas of southwest Europe: palaeogeographic and tectonic implications. Geol Soc Lond Memoirs 12(1):421–430